arXiv:1402.7125v2 [physics.atom-ph] 4 Mar 2014

Probing rotational wave-packet dynamics with the structural minimum in high-order harmonic spectra

Meiyan Qin[1,2], Xiaosong Zhu[1,2,*], Yang Li[1,2], Qingbin Zhang[1,2], Pengfei Lan[1,2], and Peixiang Lu[1,2,3]

1 Wuhan National Laboratory for Optoelectronics and School of Physics, Huazhong University of Science and Technology, Wuhan 430074, P. R. China
2 MOE Key Laboratory of Fundamental Quantities Measurement,Wuhan 430074, P. R. China

[*] *zhuxiaosong@mail.hust.edu.cn*

[3] *lupeixiang@mail.hust.edu.cn*

Abstract: We investigate the alignment-dependent high-order harmonic spectrum generated from nonadiabatically aligned molecules around the first half rotational revival. It is found that the evolution of the molecular alignment is encoded in the structural minima. To reveal the relation between the molecular alignment and the structural minimum in the high-order harmonic spectrum, we perform an analysis based on the two-center interference model. Our analysis shows that the structural minimum position depends linearly on the inverse of the alignment parameter $<\cos^2\theta>$. This linear relation indicates the possibility of probing the rotational wave-packet dynamics by measuring the spectral minima.

© 2014 Optical Society of America

OCIS codes: (190.7110) Ultrafast nonlinear optics; (190.4160) Multi-harmonic generation; (300.6560) Spectroscope, x-ray

References and links

1. J. Itatani, J. Levesque, D. Zeidler, H. Niikura, H. Pépin, J. C. Kieffer, P. B. Corkum and D. M. Villeneuve, "Tomographic imaging of molecular orbitals," Nature **432**, 867-871 (2004).
2. C. Vozzi, M. Negro, F. Calegari, G. Sansone, M. Nisoli, S. De Silvestri and S. Stagira, "Generalized molecular orbital tomography," Nature Phys, **7**, 822-826 (2011).
3. X. Zhu, M. Qin, Y. Li, Q. Zhang, Z. Xu, and P. Lu, "Tomographic reconstruction of molecular orbitals with twofold mirror antisymmetry: Overcoming the nodal plane problem," Phys. Rev. A, **87**, 045402 (2013).
4. S. Haessler, J. Caillat, W. Boutu, C. Giovanetti-Teixeira, T. Ruchon, T. Auguste, Z. Diveki, P. Breger, A. Maquet, B. Carré, R. Taïeb and P. Salières, "Attosecond imaging of molecular electronic wavepackets," Nature Phys. **6**, 200-206 (2010).
5. M. Qin, X. Zhu, Q. Zhang, and P. Lu, "Tomographic imaging of asymmetric molecular orbitals with a two-color multicycle laser field," Opt. Lett. **37**, 5208-5210 (2012).
6. R. Torres, N. Kajumba, J. G. Underwood, J. S. Robinson, S. Baker, J. W. G. Tisch, R. Nalda, W. A. Bryan, R. Velotta, C. Altucci, I. C. E. Turcu, and J. P. Marangos, "Probing orbital structure of polyatomic molecules by high-Order harmonic generation," Phys. Rev. Lett. **98**, 203007 (2007).
7. X. Zhu, Q. Zhang, W. Hong, P. Lu, and Z. Xu, "Laser-polarization-dependent photoelectron angular distributions from polar molecules," Opt. Express **19**, 24198-24209 (2011).
8. Q. Liao, Y. Zhou, C. Huang, and P. Lu, "Multiphoton Rabi oscillations of correlated electrons in strong-field nonsequential double ionization," New J. Phys. **14**, 013001 (2012).
9. R. Torres, R. de Nalda, and J. P. Marangos, "Dynamics of laser-induced molecular alignment in the impulsive and adiabatic regimes: A direct comparison," Phys. Rev. A **72**, 023420 (2005).

10. J. Ortigoso and M. Rodriguez, M. Gupta and B. Friedrich, "Time evolution of pendular states created by the interaction of molecular polarizability with a pulsed nonresonant laser field," J. Chem. Phys. **110**, 3870-3875 (1999).
11. T. Seideman, "Revival Structure of Aligned Rotational Wave Packets," Phys. Rev. Lett. **83**, 4971-4974 (1999).
12. M. Machholm and N. E. Henriksen, " Field-Free Orientation of Molecules," Phys. Rev. Lett. **87**, 193001 (2001).
13. F. Rosca-Pruna and M. J. J. Vrakking, "Experimental Observation of Revival Structures in Picosecond Laser-Induced Alignment of I_2," Phys. Rev. Lett. **87**, 153902 (2001).
14. H. Stapelfeldt and T. Seideman, "Aligning molecules with strong laser pulses," Rev. Mod. Phys. **75**, 543-557 (2003).
15. N. Xu, C. Wu, J. Huang, Z. Wu, Q. Liang, H. Yang, and Q. Gong, "Field-free alignment of molecules at room temperature," Opt. Express, **14**, 4992-4997 (2006).
16. R. A. Bartels, T. C. Weinacht, N. Wagner, M. Baertschy, C. H. Greene, M. M. Murnane, and H. C. Kapteyn, "Phase modulation of ultrashort light pulses using molecular rotational wave packets," Phys. Rev. Lett. **88**, 013903 (2001).
17. K. F. Lee, D. M. Villeneuve, P. B. Corkum, and E. A. Shapiro, "Phase control of rotational wave packets and quantum information," Phys. Rev. Lett. **93**, 233601 (2004).
18. K. Miyazaki, M. Kaku, G. Miyaji, A. Abdurrouf, and F. H. M. Faisal, "Field-Free Alignment of Molecules Observed with High-Order Harmonic Generation," Phys. Rev. Lett. **95**, 243903 (2005).
19. T. Kanai, S. Minemoto and H. Sakai, "Quantum interference during high-order harmonic generation from aligned molecules," Nature **435**, 470-474 (2005).
20. M. Lewenstein, Ph. Balcou, M. Yu. Ivanov, A. L'Huillier, and P. Corkum, "Theory of high-harmonic generation by low-frequency laser fields," Phys. Rev. A **49,** 2117-2132 (1994).
21. M. Qin, X. Zhu, Q. Zhang, W. Hong, and P. Lu, "Broadband large-ellipticity harmonic generation with polar molecules," Opt. Express **19**, 25084-25092 (2011).
22. A. Rupenyan, P. M. Kraus, J. Schneider, and H. J. Wörner, "High-harmonic spectroscopy of isoelectronic molecules: Wavelength scaling of electronic-structure and multielectron effects," Phys. Rev. A **87**, 033409 (2013).
23. M. J. Frisch, G. W. Trucks, H. B. Schlegel, G. E. Scuseria, M. A. Robb, J. R. Cheeseman, J. A. Montgomery Jr., T. Vreven, K. N. Kudin, J. C. Burant, J. M. Millam, S. S. Iyengar, J. Tomasi, V. Barone, B. Mennucci, M. Cossi, G. Scalmani, N. Rega, G. A. Petersson, H. Nakatsuji,M. Hada,M. Ehara, K. Toyota, R. Fukuda, J. Hasegawa,M. Ishida, T. Nakajima, Y. Honda, O. Kitao, H. Nakai, M. Klene, X. Li, J. E. Knox, H. P. Hratchian, J. B. Cross, V. Bakken, C. Adamo, J. Jaramillo, R. Gomperts, R. E. Stratmann, O. Yazyev, A. J. Austin, R. Cammi, C. Pomelli, J. W. Ochterski, P. Y. Ayala, K. Morokuma, G. A. Voth, P. Salvador, J. J. Dannenberg, V. G. Zakrzewski, S. Dapprich, A. D. Daniels, M. C. Strain, O. Farkas, D. K. Malick, A. D. Rabuck, K. Raghavachari, J. B. Foresman, J. V. Ortiz, Q. Cui, A. G. Baboul, S. Clifford, J. Cioslowski, B. B. Stefanov, G. Liu, A. Liashenko, P. Piskorz, I. Komaromi, R. L. Martin, D. J. Fox, T. Keith, M. A. Al-Laham, C. Y. Peng, A. Nanayakkara, M. Challacombe, P. M. W. Gill, B. Johnson, W. Chen, M. W. Wong, C. Gonzalez, and J. A. Pople, Gaussian 03, Revision C.02, Gaussian Inc., Wallingford, CT (2010).
24. G. Cerullo and S. D. Silvestri, "Ultrafast optical parametric amplifiers," Rev. Sci. Instrum. 74, 1-18 (2003).
25. Q. Zhang, E. J. Takahashi, O. D. Mücke, P. Lu, and K. Midorikawa, "Dual-chirped optical parametric amplification for generating few hundred mJ infrared pulses," Opt. Express **19**, 7190-7212 (2011).
26. C. Jin, A. T. Le, and C. D. Lin, "Analysis of effects of macroscopic propagation and multiple molecular orbitals on the minimum in high-order harmonic generation of aligned CO_2," Phys. Rev. A **83**, 053409 (2011).
27. A. T. Le, R. R. Lucchese, S. Tonzani, T. Morishita, and C. D. Lin, "Quantitative rescattering theory for high-order harmonic generation from molecules," Phys. Rev. A **80**, 013401 (2009).
28. M. Lein, N. Hay, R. Velotta, J. P. Marangos, and P. L. Knight, "Interference effects in high-order harmonic generation with molecules," Phys. Rev. A. **66**, 023805 (2002).
29. X. Zhu, Q. Zhang, W. Hong, P. Lan, and P. Lu, "Two-center interference in high-order harmonic generation from heteronuclear diatomic molecules," Opt. Express **19**, 436-447 (2010).
30. S. J. Weber, M. Oppermann, and J. P. Marangos, "Role of rotational wave packet in strong field experiments," Phys. Rev. Lett. **111**, 263601 (2013).

1. Introduction

The main impetus to the development of strong field physics is measuring and understanding the electronic structure and dynamics of matter on its natural timescale [1–8]. When measuring the electronic structure and dynamics for molecules, the pre-alignment of the target molecules is required. This can be adiabatically or nonadiabatically achieved by using moderately intense laser pulses [9–11]. Generally, the nonadiabatic alignment is preferred because it can produce macroscopic ensembles of highly aligned molecules under the field-free condition. The mech-

anism of the field-free alignment is well understood by the rephasing of the rotational wave packet [11, 12]. In detail, the target molecules are impulsively excited by an intense ultrashort laser pulse into a broad superposition of field-free rotational states. After the alignment pulse is turned off, the excited wave packet will evolve under the field-free condition and rephase to form a revival at certain time delays. The revival structure in the nonadiabatic alignment was first observed with the Coulomb explosion imaging by Rosca-Pruna and Vrakking [13]. Since then, the fundamental behavior and dynamics of the alignment have been extensively studied using the Coulomb explosion imaging and polarization spectroscopy [14, 15]. The investigation of nonadiabatic alignment is motivated by several intriguing applications including the use of alignment revivals to compress laser pulse [16], the phase control of rotational wave packets [17], and its use to follow the time evolution of the electron wave packets [4].

Recently it was demonstrated that the revival structure of nonadiabatic alignment of molecules can also be observed via the high-order harmonic generation (HHG) [18, 19]. Therein, the evolution of the alignment parameter is imprinted in the change of the harmonic yield with the delay between the harmonic generating pulse and the alignment pulse. The modulation due to the rotational dynamics, however, is influenced by the symmetry of the molecules and the quantum interference in the HHG. This may complicate the extraction of the information about the rotational dynamics. In this paper, we theoretically investigate the alignment-dependent spectral minimum in HHG from nonadiabatically aligned CO_2, N_2, N_2O and CO molecules, around their first half rotational revivals. It is found that the alignment-dependent structural minimum presents a similar temporal behavior to that of the alignment parameter $<\cos^2\theta>$ (i.e. the expectation value of $\cos^2\theta$ where θ is the angle between the molecular axis and the field direction) and this phenomenon is not influenced by the change of the wavelength and intensity of the probe pulse. To reveal the implication of the phenomenon, we perform an analysis based on the two-center interference model and find that the structural minimum position depends linearly on the inverse of the alignment parameter. As the molecular rotational dynamics is well characterized by the evolution of $<\cos^2\theta>$, our results indicate the possibility of tracing the molecular rotational dynamics by measuring the spectral minimum.

2. Theoretical model

In our simulation, we use the strong-field approximation (SFA) model for molecules [20, 21] to calculate the HHG spectrum for a fixed alignment. Within the single active electron (SAE) approximation, the time-dependent dipole velocity is given by

$$\begin{aligned}\mathbf{v}_{dip}(t;\theta) &= i\int_{-\infty}^{t} dt' \left[\frac{\pi}{\zeta + i(t-t')/2}\right]^{\frac{3}{2}} \exp[-iS_{st}(t',t)] \\ &\times \mathbf{F}(t')\cdot\mathbf{d}_{ion}\left[\mathbf{p}_{st}(t',t)+\mathbf{A}(t');\theta\right] \\ &\times \mathbf{v}^{*}_{rec}\left[\mathbf{p}_{st}(t',t)+\mathbf{A}(t);\theta\right] + c.c.. \end{aligned} \quad (1)$$

In this equation, ζ is a positive constant. t' and t correspond to the ionization and recombination time of the electron, respectively. θ is the alignment angle between the molecular axis and the polarization of the probe pulse. $\mathbf{F}(t)$ refers to the electric field of the probe pulse, and $\mathbf{A}(t)$ is its associated vector potential. $\mathbf{p}_{st}$ and S_{st} are the stationary momentum and the quasi-classical action, which are given by

$$\mathbf{p}_{st}(t',t) = -\frac{1}{t-t'}\int_{t'}^{t}\mathbf{A}(t'')dt'' \quad (2)$$

and

$$S_{st}(t',t) = \int_{t'}^{t}\left(\frac{[\mathbf{p}_{st}+\mathbf{A}(t'')]^2}{2}+I_p\right)dt'' \quad (3)$$

with I_p being the ionization energy of the molecular state that the electron is ionized from. $\mathbf{d}_{ion}[p;\theta]$ and $\mathbf{v}_{rec}[p;\theta]$ are the dipole matrix elements describing the ionization and recombination of the electron, respectively. Within the SFA model, the re-colliding wave packet is approximately described by the plane wave. Hence the dipole matrix elements are given by

$$\mathbf{d}_{ion}[p;\theta] = \langle \Psi_0(x,y,z;\theta)|\vec{r}|\Psi_p\rangle, \tag{4}$$

$$\mathbf{v}_{rec}[p;\theta] = \langle \Psi_0(x,y,z;\theta)|-i\nabla_r|\Psi_p\rangle, \tag{5}$$

with $\Psi_p = \exp(i\vec{p}\cdot\vec{r})$ being the electronic continuum state and $\Psi_0(x,y,z;\theta)$ being the ground state of the target molecule. After the time-dependent dipole velocity is obtained, the complex amplitude of the high-order harmonics with a frequency ω_n is calculated by

$$\tilde{\mathbf{E}}(\omega_n;\theta) = \int e^{i\omega_n t}\frac{d}{dt}\mathbf{v}_{dip}(t;\theta)dt. \tag{6}$$

Coherently superposing the high-order harmonic emissions at different alignment angles weighted by the angular distribution, the spectrum at the delay τ with respect to the pump pulse is obtained

$$S(\omega_n;\tau) = |\int E(\omega_n;\theta)exp[iP(\omega_n;\theta)]\rho(\theta;\tau)d\theta|^2. \tag{7}$$

Here, $E(\omega_n;\theta) = |\tilde{\mathbf{E}}(\omega_n;\theta)|$ and $P(\omega_n;\theta) = \arg(\tilde{\mathbf{E}}(\omega_n;\theta))$ are the amplitude and phase of the high-order harmonics generated from the molecule aligned at θ. $\rho(\theta;\tau)$ is the angular distribution multiplied by $\sin\theta$ and is given by

$$\rho(\theta;\tau) = \sin\theta(1/Z)\sum_{J_i}Q(J_i)\sum_{M_i=-J_i}^{J_i}\int|\Psi^{J_iM_i}(\theta,\phi;\tau)|^2d\phi. \tag{8}$$

Here $Q(J_i) = g_{J_i}\exp(-BJ_i(J_i+1)/(k_BT))$ is the Boltzmann distribution function of the initial field-free state $|J_i,M_i\rangle$ at temperature T, $Z = \sum_{J=0}^{J_{max}}(2J+1)Q(J)$ is the partition function, k_B and B are the Boltzmann constant and the rotational constant of the molecule, respectively. g_{J_i} is introduced to include the different population of the initial J-states that arises from the nuclear-spin statistics. For CO_2, only even-J states are populated. For N_2, the population ratio between the even- and odd-J states is 2:1, while for N_2O and CO, the population ratio is 1:1. $\Psi^{J_iM_i}(\theta,\phi;\tau)$ is the rotational wave packet excited from the initial state $|J_i,M_i\rangle$, and is obtained by solving the time-dependent Schrödinger equation (TDSE) within the rigid-rotor approximation [10, 11]

$$i\frac{\partial\Psi(\theta,\phi;\tau)}{\partial\tau} = [B\mathbf{J}^2 - \frac{E_p(\tau)^2}{2}(\alpha_\parallel\cos^2\theta + \alpha_\perp\sin^2\theta)]\Psi(\theta,\phi;\tau). \tag{9}$$

In this equation, $\alpha_\parallel$ and $\alpha_\perp$ are the polarizabilities in parallel and perpendicular directions with respect to the molecular axis, respectively. $E_p(\tau)$ represents the electric field of the alignment pulse. The degree of alignment is characterized by the alignment parameter $<\cos^2\theta>$, and is given by

$$<\cos^2\theta>(\tau) = (1/Z)\sum_{J_i}Q(J_i)\sum_{M_i=-J_i}^{J_i}\langle\Psi^{J_iM_i}(\theta,\phi;\tau)|\cos^2\theta|\Psi^{J_iM_i}(\theta,\phi;\tau)\rangle. \tag{10}$$

3. Result and discussion

In our simulation, linearly polarized alignment and probe pulses are used, with their polarization directions parallel to each other. In order to obtain a broadband spectrum to observe the spectral minimum, the long-wavelength probe pulses are used. Under these conditions, the influence of the multi-channel contribution is small [22] and can be neglected. Therefore only the ionization channel involving the highest occupied molecular orbital (HOMO) of the target is considered in our simulation. Using Eqs. (1-6), the HHG spectrum for a fixed alignment is calculated. The involved molecular orbital is calculated by using the Gaussian 03 *ab initio* code [23] with the 6-311G basis set for the CO_2, CO, N_2O molecules and with the 3-21G basis set for the N_2 molecule. The rotational wave packet excited by the alignment pulse is calculated by solving Eq. (9). According to the rigid-rotor model, the rotational period of molecules is determined by $T_r = 1/(2Bc)$, with B and c being the rotational constant and the speed of the light, respectively. In Table 1, the molecular parameters of the CO_2, N_2, N_2O, and CO molecules used in the alignment calculation are listed.

TABLE 1: The molecular parameters of the CO_2, N_2, N_2O, and CO molecules

Molecule	B (cm^{-1})	$\alpha_{\parallel} - \alpha_{\perp}$ (a.u.)	$\alpha_{\perp}$ (a.u.)	T_r (ps)
CO_2	0.389	15.4	14.7	42.7
N_2	2.01	6.276	9.785	8.26
N_2O	0.41	18.85	13.16	40.5
CO	1.93	3.536	11.83	8.6

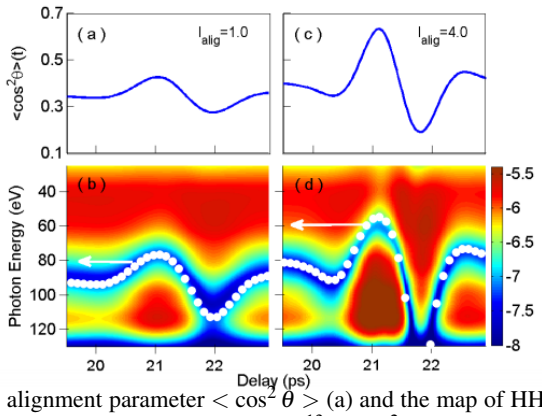

Fig. 1. (a-b) The alignment parameter $< \cos^2\theta >$ (a) and the map of HHG spectra (b) for the alignment pulse with an intensity of 1.0×10^{13} W/cm^2. (c-d) The alignment parameter $< \cos^2\theta >$ (c) and the map of HHG spectra (d) for the alignment pulse with an intensity of 4.0×10^{13} W/cm^2. The same probe pulse is used to obtain the two spectral maps. The vertical axis representing the photon energy is upside-down. The calculated photon energy of the spectral minimum is shown by the white dots. The horizontal and vertical axes are the same as those for the map of the HHG spectra.

We first simulate the alignment-dependent HHG spectrum generated from CO_2 molecule. In Figs. 1(a) and 1(b), the evolution of the alignment parameter $< \cos^2\theta >$ around the first half revival (panel a) and the corresponding map of the HHG spectrum as a function of the time delay and the photon energy (panel b) are presented. For the map of the HHG spectrum (panel b), the horizontal axis represents the time delay with respect to the alignment pulse, and the vertical axis represents the photon energy of the high-order harmonics. Here, an 800 nm, 100 fs alignment pulse with an intensity of 1.0×10^{13} W/cm^2 is used. The rotational temperature is set to be 40 K. The wavelength, pulse duration, and intensity of the probe pulse used to generate

high-order harmonics are 1450 nm, 18 fs, and 1.7×10^{14} W/cm^2, respectively. In experiment, this IR pulse can be produced by optical parametric amplification (OPA) technology based the wavelength down-conversion of Ti:sapphire laser source [24, 25]. As shown in Fig. 1(b), obvious spectral minimum is observed in the HHG spectrum at every time delay. Moreover, the alignment-dependent spectral minimum has a similar shape to that of the evolution of $< \cos^2\theta >$. In detail, when the value of $< \cos^2\theta >$ increases (or decreases), the spectral minimum position correspondingly shifts to lower (or higher) photon energy [22, 26]. The lowest and highest photon energy of the spectral minima appear at the delays when $< \cos^2\theta >$ reaches its maximum and minimum, respectively. For a further investigation, we also study the cases where the molecular alignment is achieved by using the pulses with different intensities. The results for the 4.0×10^{13} W/cm^2 alignment pulse are presented in the second column of Fig. 1. As shown in Figs. 1(c) and 1(d), the evolution of the spectral minimum also presents a similar shape to that of $< \cos^2\theta >$. In this case, the maximum of $< \cos^2\theta >$ is around 0.6. The corresponding spectral minimum is observed around 60.5 eV, which differs from the measurements in Ref. [22] by about 13 eV (close to the ionization energy of CO_2 molecule). The disagreement arises from the plane-wave approximation of the electronic continuum state in the SFA [4]. This is improved in the quantitative re-scattering (QRS) theory by employing a more precise transition dipole with scattering wave instead of the plane wave for the recombination step in a HHG process [27]. As shown in Figs. 1(a) and 1(c), when varying the intensity of the alignment pulse, not only the amplitude but also the shape of $< \cos^2\theta >$ are changed. The corresponding changes in the evolution of the spectral minimum are also observed, as shown in Figs. 1(b) and 1(d). Hence, the shape of the alignment-dependent spectral minimum varies with that of $< \cos^2\theta >$.

In the following, we investigate the role of the probe pulse in the phenomenon observed in Fig. 1. The maps of the harmonic spectrum produced by two different probe pulses are displayed in Fig. 2. The wavelength and intensity of the two probe pulses are different, which are indicated in the corresponding maps of the high-order harmonic spectrum. The same alignment

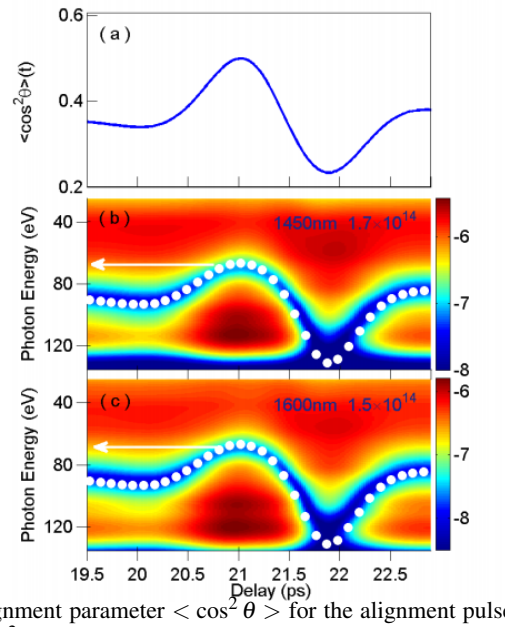

Fig. 2. (a) The alignment parameter $< \cos^2\theta >$ for the alignment pulse with an intensity of 2.0×10^{13} W/cm^2. (b-c) The maps of the HHG spectra produced by two different probe pulses. The calculated photon energy of the spectral minimum is shown by the white dots. The horizontal and vertical axes are the same as those for the maps of the HHG spectra.

pulse with an intensity of 2.0×10^{13} W/cm^2 is used for the two maps. The alignment parameter $<\cos^2\theta>$ is presented in Fig. 2(a). Other parameters of the alignment and probe pulses are the same as those used for Fig. 1. As shown in Fig. 2, the shapes of the spectral minimum for the two different probe pulses are the same, and simultaneously similar to that of $<\cos^2\theta>$. Therefore, the imprint of $<\cos^2\theta>$ on the alignment-dependent spectral minimum is not influenced by the changing of the wavelength and intensity of the probe pulse.

To get an insight into the relation between the spectral minimum and the alignment parameter $<\cos^2\theta>$, we perform an analysis based on the two-center interference model [19,28,29]. According to this model, the condition for the interference minimum is $R\cos\theta = n\lambda$ for molecules with an anti-bounding symmetric HOMO. Here λ is the de Broglie wavelength of the returning electron, R is the internuclear distance of the target molecule, and n is a positive integer. According to the relationship $\omega = \frac{k^2}{2} + I_p$ with the electron momentum $k = \frac{2\pi}{\lambda}$ (atomic units are used), one can obtain $\omega = \frac{2\pi^2}{R^2\cos^2\theta} + I_p$, where ω and I_p are the photon energy of the interference minimum and the ionization energy of the target molecule, respectively. The above formula is derived based on the responses of the molecules aligned at a fixed angle. After taking into account the partial alignment, this relation between the minimum position and $\cos^2\theta$ can still remain, i.e. $\tilde{\omega} = \frac{2\pi^2}{R^2}\frac{1}{<\cos^2\theta>} + I_p$. Here, $\tilde{\omega}$ represents the minimum position in the high-order harmonic spectrum generated from partially aligned molecules, $<\cos^2\theta>$ is the alignment parameter. As for the molecule with a bounding symmetric HOMO, the similar formula is given by $\tilde{\omega} = \frac{\pi^2}{2R^2}\frac{1}{<\cos^2\theta>} + I_p$. We apply the above formula to the CO_2 molecule, whose HOMO possesses anti-bounding symmetry, and calculate the photon energy of the spectral minimum

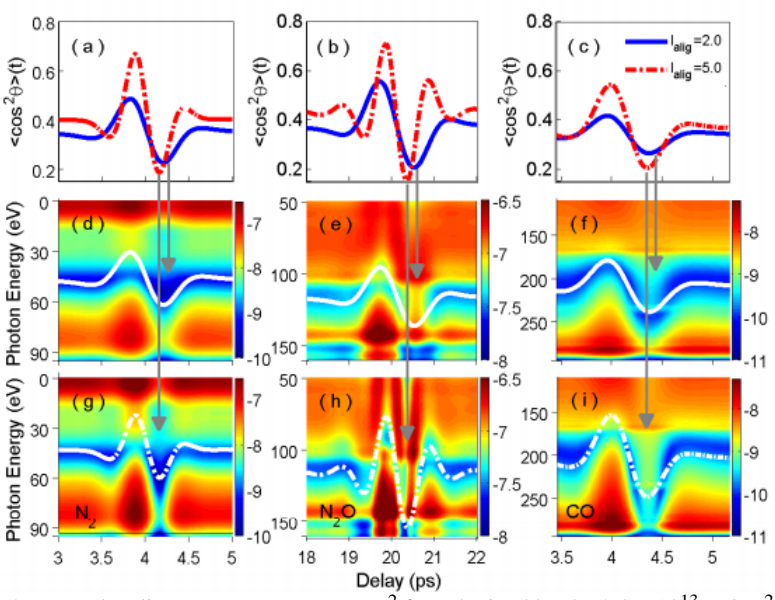

Fig. 3. (a-c) The alignment parameter $<\cos^2\theta>$ obtained by the 2.0×10^{13} W/cm^2 (blue solid line) and 5.0×10^{13} W/cm^2 (red dash-dotted line) alignment pulse. (d-f) The maps of the high-order harmonic spectra for the 2.0×10^{13} W/cm^2 alignment pulse. (g-i) The maps of the high-order harmonic spectra for the 5.0×10^{13} W/cm^2 alignment pulse. The first, second, and third columns present the results for N_2, N_2O and CO molecules, respectively. For clarity, the curves of $<\cos^2\theta>$ are depicted by the white solid line for the 2.0×10^{13} W/cm^2 alignment pulse and by the white dash-dotted line for the 5.0×10^{13} W/cm^2 alignment pulse on the corresponding maps of the high-order harmonic spectra.

with the value of $< \cos^2\theta >$. The results are presented by the white dots in Fig. 1 and Fig. 2. The horizontal and vertical axes are the same as those for the map of the high-order harmonic spectrum. As shown by the white dots in Fig. 1 and Fig. 2, the calculated photon energy of the spectral minimum agrees well with that observed in the high-order harmonic spectrum. Hence the alignment-dependent spectral minimum position is well reproduced by the formula with $< \cos^2\theta >$ and depends linearly on the inverse of the alignment parameter $\frac{1}{<\cos^2\theta>}$.

To explore the universality of the phenomenon observed in the CO_2 molecule, we investigate the alignment-dependent spectral minimum of N_2, N_2O and CO molecules that possess different orbital symmetry. For each molecule, two alignment pulses with different intensities, i.e. 2.0×10^{13} W/cm^2 and 5.0×10^{13} W/cm^2, are considered. Other parameters of the alignment pulses and the rotational temperature are the same as those used in Fig. 1 and Fig. 2. In the case of N_2 molecule, a 1600 nm, 20 fs probe pulse with an intensity of 0.9×10^{14} W/cm^2 is used. For N_2O molecule, the wavelength, pulse duration, and intensity of the probe pulse are 2000 nm, 15 fs, and 1.2×10^{14} W/cm^2, respectively. In the CO molecule case, because the spectral minimum occurs at higher photon energy [29], a probe pulse with a longer wavelength is used. The wavelength, pulse duration, and intensity are 2500 nm, 25 fs, and 1.5×10^{14} W/cm^2, respectively. In our simulation, few-cycle long-wavelength probe pulses with low intensities are used for all the molecules. Hence the influence of the multi-channel contribution in HHG is small and can be neglected [2, 22].

In Figure. 3, the alignment parameter $< \cos^2\theta >$ and the corresponding maps of the high-order harmonic spectrum for N_2, N_2O and CO molecules are presented in the first, second, and third columns, respectively. From Fig. 3, one can see that, similar to the case of CO_2 molecule, the evolution of the alignment parameter $< \cos^2\theta >$ is also imprinted in the corresponding spectral minimum for the three molecules. The temporal behavior of the spectral minimum varies with that of $< \cos^2\theta >$. For clarity, the curves of $< \cos^2\theta >$ are depicted by the white lines in the corresponding maps of the high-order harmonic spectrum. As shown in the second and third rows of Fig. 3, the white lines representing $< \cos^2\theta >$ and the minimum position have similar temporal behavior. One can also see that the white lines do not always match the position of the spectral minimum, which is very obvious in the case of the stronger degrees of alignment shown in Figs. 3(g-i). These deviations are due to the fact that the spectral minimum position depends linearly on $\frac{1}{<\cos^2\theta>}$ rather than $< \cos^2\theta >$, which will be demonstrated in Fig. 4. Compared with the cases of the N_2 and CO molecules shown in the first and third columns of Fig. 3, the structures of the high-order harmonic spectral maps of N_2O molecule shown in the second column of Fig. 3 are more complicated and the spectral minimum is difficult to identify. As demonstrated in the recent work [30], this is due to the intricate evolution of the rotational wave packet shown in Fig. 3(b) and the complicated structure of the recombination dipole.

We then apply the formulae derived from two-center interference model to the N_2, N_2O and CO molecules. Whereas the calculated spectral minimum positions do not agree well with those observed in the high-order harmonic spectral maps (the results are not shown here). This is because for N_2 molecule, its HOMO exhibits a strong mixing between *s* and *p* states, while for N_2O and CO molecules with nonsymmetric orbitals, the components of the HOMO become more complicated. As a result, the spectral minimum position before taking into account the partial alignment does not exactly agree with that predicted by the two-center interference model. Hence, the formulae can not quantitatively describe the relation between the minimum position and the alignment parameter. Even so, the linear relation between $\tilde{\omega}$ and $\frac{1}{<\cos^2\theta>}$ still remains with the two linear coefficients to be determined, considering the similarity of the temporal behavior between the spectral minimum position and $< \cos^2\theta >$ also observed in the cases of the N_2, N_2O and CO molecules. To determine the two linear coefficients, we fit the spectral minimum positions observed in the maps of the high-order harmonic spectrum shown

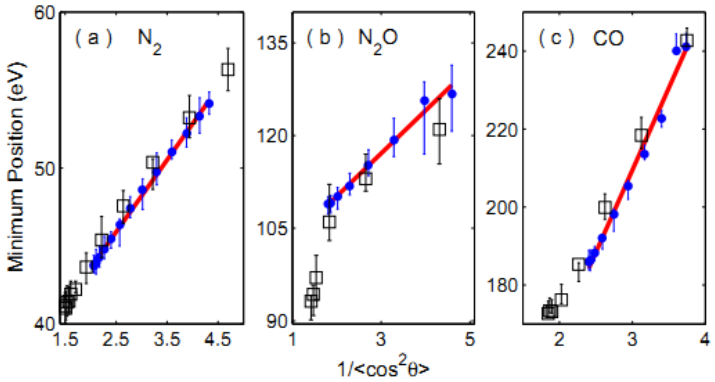

Fig. 4. The extracted spectral minimum positions from the second (the blue dots) and third (the black squares) rows of Fig. 3 and the corresponding least-square fits (red solid line) for the N_2 (panel a), N_2O (panel b) and CO (panel c) molecules. The horizontal axis represents the inverse of the alignment parameter.

in the second row of Fig. 3, through the linear least-squares fitting method. The results are presented in Fig. 4 for N_2 (panel a), N_2O (panel b) and CO (panel c). The minimum positions extracted from the second and third rows of Fig. 3 are presented by the blue dots and the black squares, respectively. The error bars of the data points, which describes how well the spectral minimum can be defined from Fig. 3, are also depicted. As shown in Fig. 4, the extracted spectral minima from the second row of Fig. 3 are well fitted by a linear function of $\frac{1}{<\cos^2\theta>}$ for the three molecules. Furthermore, for the N_2 and CO molecules, the minimum positions extracted from the third row of Fig. 3 follow the same linear function of $\frac{1}{<\cos^2\theta>}$ as those extracted from the second row of Fig. 3. As for the N_2O molecule, however, the spectral minimum position for the stronger degree of alignment does not follow the same function of $\frac{1}{<\cos^2\theta>}$ as those extracted from Fig. 3(e). The relationship between the minimum position and $\frac{1}{<\cos^2\theta>}$ is even not linear, as shown by the black squares in Fig. 4(b). This is because the HOMO of the N_2O molecule is contributed by three atoms, which may complicate the relationship between the spectral minimum position and $\frac{1}{<\cos^2\theta>}$. Therefore, when the molecular orbital is contributed by two atomic centers, the structural minimum position $\tilde{\omega}$ depends linearly on the inverse of the alignment parameter $\frac{1}{<\cos^2\theta>}$. The linear coefficients are independent on the alignment and probe pulses, as shown in Figs. 1, 2 and 4. Hence, after determining the linear coefficients for the target molecules, the formula can be used to trace the evolution of $<\cos^2\theta>$ with the measured structural minima in the experiments using various alignment and probe pulses. As the molecular rotational wave-packet dynamics is well characterized by the alignment parameter $<\cos^2\theta>$, one can trace the rotational wave-packet dynamics by measuring the alignment-dependent spectral minima. Compared with the Coulomb explosion imaging, our method can realize all-optical measurement of the angular distribution without destroying the molecules and can directly trace the value of $<\cos^2\theta>$ through a simple formula of the spectral minimum. The precision of tracing the rotational dynamics with our method depends on the identification of the minimum position. When the spectral minimum is difficult to identify, correspondingly, it will be difficult to precisely trace the rotational dynamics.

4. Conclusion

In summary, we investigate the dependence of the spectral minimum position on the alignment parameter $<\cos^2\theta>$ around the first half rotational revival for the CO_2, N_2, N_2O and

CO molecules. It is found that the alignment-dependent spectral minimum presents a similar temporal behavior to that of $< \cos^2 \theta >$. Our analysis shows that the minimum position depends linearly on the inverse of $< \cos^2 \theta >$. For the molecular orbitals contributed by two atomic centers, the two linear coefficients are independent on the alignment and probe pulses. As the molecular rotational dynamics is well characterized by the evolution of $< \cos^2 \theta >$, it is possible to probe the rotational wave-packet dynamics by measuring the alignment-dependent spectral minima.

Acknowledgment

This work was supported by the NNSF of China under Grants No. 11234004 and 61275126, the 973 Program of China under Grant No. 2011CB808103 and the Doctoral fund of Ministry of Education of China under Grant No. 20100142110047.